Eur. Phys. J. A **27**, 301–312 (2006)
DOI 10.1140/epja/i2006-10007-y

THE EUROPEAN PHYSICAL JOURNAL A

Gamma-ray spectroscopy of the nucleus ^{139}Ce

D. Bucurescu[a], G. Căta-Danil, I. Căta-Danil, M. Ivaşcu, N. Mărginean, R. Mărginean, L.C. Mihăilescu, C. Rusu, and G. Suliman

Horia Hulubei National Institute of Physics and Nuclear Engineering, P.O. Box MG-6, R-76900 Bucharest, Romania

Received: 6 February 2006 / Revised version: 9 March 2006 /
Published online: 18 April 2006 –
Communicated by D. Schwalm

Abstract. Gamma-ray coincidence techniques are used to determine new level structures in the $N = 81$ nucleus ^{139}Ce, at low spins and excitation energies with the ^{139}La(p, nγ) reaction at 5.0 and 6.0 MeV incident energy, and at high spins with the ^{130}Te(^{12}C, 3nγ) reaction at 50.5 MeV, respectively. Lifetime determinations are also made in the (p, nγ) reaction with the centroid DSA method. The observed level structures are discussed by comparison with existing calculations and with those in the neighbouring nucleus ^{140}Ce.

PACS. 21.10.-k Properties of nuclei; nuclear energy levels – 23.20.Lv gamma transitions and level energies – 27.60.+j $90 \leq A \leq 149$

1 Introduction

Both the complete spectroscopy at low spin and excitation energies, and the study of high-spin states in the $N = 81$ nucleus ^{139}Ce are of interest in order to enrich our knowledge in the vicinity of the $N = 82$ magic number. The low-lying states of ^{139}Ce have been previously studied [1] through the beta decay of ^{139}Pr [2], as well as with reactions with light projectiles. A (p, nγ) reaction study has been performed prior to our present investigation [3], but without coincidence measurements so that excited levels have been assigned tentatively. Neutron-hole states in the closed-shell nucleus ^{140}Ce have been investigated through the (p, d), (^{3}He, α), and (d, t) reactions [4]. Higher-spin states have been studied with (α, xnγ) reactions [5,6].

At low excitation energy, the $^{139}_{58}$Ce$_{81}$ nucleus is expected to have an important number of states resulting from the coupling of single neutron-hole states to the phonon vibrations of the neighbouring even-even core. The (p, n) reaction in the sub-Coulomb region is a compound nuclear process, therefore a non-selective reaction. It is expected to excite practically all these states in the residual nucleus, within a certain spin window, regardless of their structural configuration. The present (p, nγ) reaction experiment has been initiated with the purpose to excite ^{139}Ce levels with low spin and excitation energy, thus making an attempt towards a more complete level scheme in this region. Level lifetimes have also been determined in this experiment with the Doppler shift attenuation method.

[a] e-mail: bucurescu@tandem.nipne.ro

In addition, an experiment with the ^{130}Te(^{12}C, 3nγ) reaction extends the results of the previous (α, xn) and (^{3}He, xn) reactions in the high-spin region ($I \geq 11/2$), thus enriching the systematics of the nuclear-structure evolution along the $N = 81$ chain.

The next two sections present the two experiments performed and the results (level schemes) obtained, and the final section contains a discussion of these results and the conclusions.

2 Experimental techniques and results

2.1 The ^{139}La(p, nγ)^{139}Ce reaction study

For this experiment proton beams with energies of 5.0 and 6.0 MeV and currents of 10–15 nA have been delivered by the FN tandem Van de Graaff accelerator of our Institute. The target was a foil of natural Lantanum (99.91% in ^{139}La), 20 mg/cm^2 thick. Two types of measurements have been made. First, at 6.0 MeV incident energy, two HPGe detectors of about 25% relative efficiency have been placed at 90° and 125° with respect to the beam direction and at 9 cm distance from the target, and a one litre NE213 liquid scintillator detector (for neutron detection) was placed at 0°. Coincidences between these three detectors have been recorded in the event mode and later sorted off-line. The neutron-gamma discrimination has been achieved with the pulse shape analysis technique. In the off-line analysis, different coincidence matrices have been produced. Thus, for the neutron–γ-ray coincidences, the matrix had the n-γ discrimination spectrum on one axis and the γ-ray energy on the other axis. For the γ-γ coincidences we produced

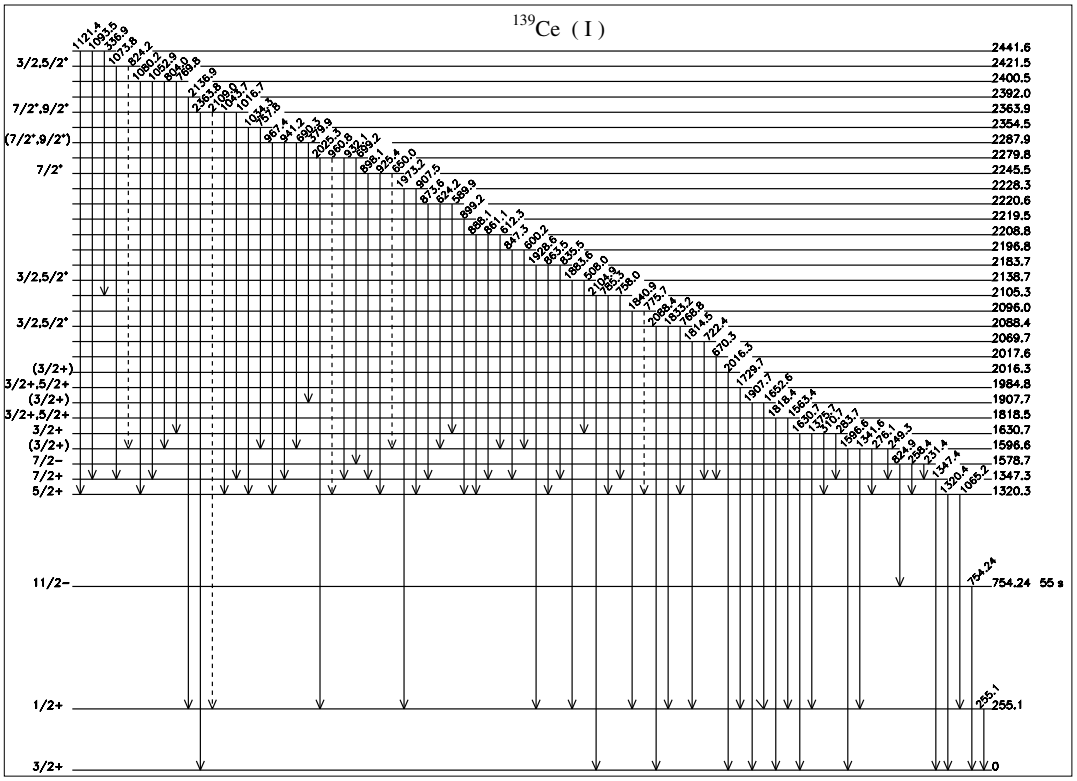

Fig. 1. Levels of ^{139}Ce (up to 2.44 MeV excitation) and their gamma-ray decay, as observed in the present (p, nγ) reaction study.

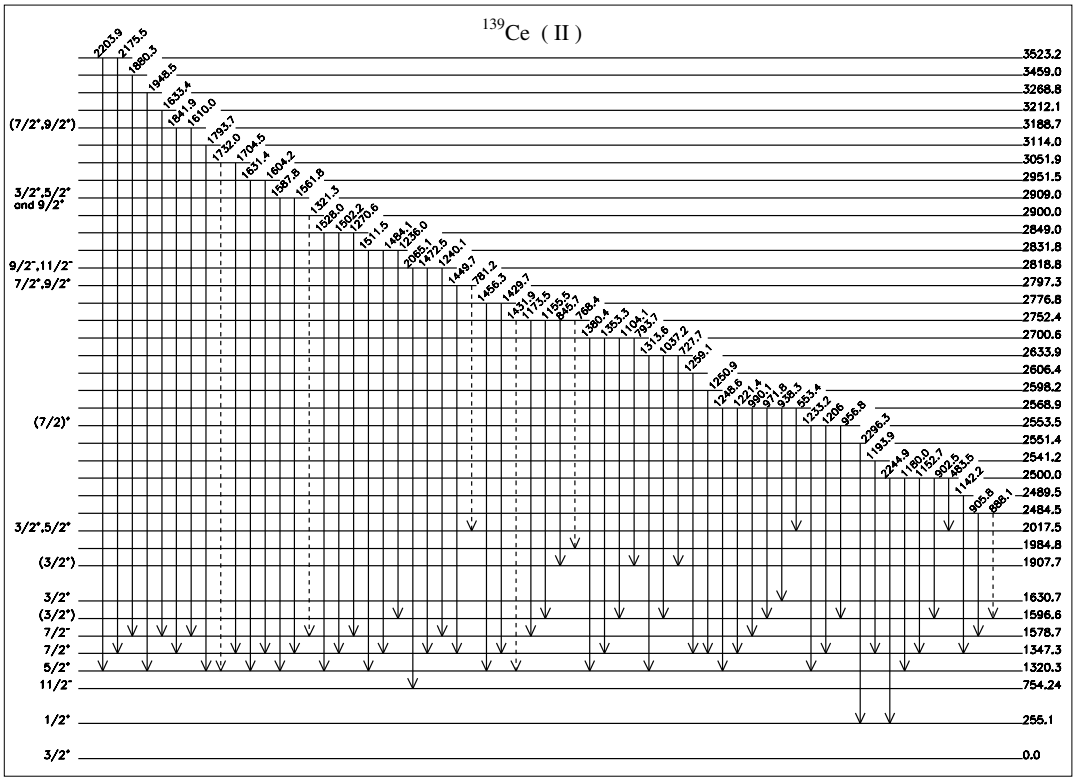

Fig. 2. Same as fig. 1, but for levels above 2.44 MeV excitation.

Table 1. List of gamma rays observed in the ^{139}La(p, nγ)^{139}Ce reaction with their placement into the level scheme, their relative intensities and angular-distribution coefficients.

E_γ (keV)	E_i (keV)	E_f (keV)	I_γ	A_2/A_0	A_4/A_0
231.4	1578.7	1347.3	2.04(122)		
249.3	1596.6	1347.3	<0.10		
255.1	255.1	0.0	59.6(44)		
258.4	1578.7	1320.3	7.60(40)		
276.1	1596.6	1320.3	5.05(19)	0.02(14)	−0.10(18)
283.7	1630.7	1347.3	0.33(12)		
310.7	1630.7	1320.3	0.15(43)		
336.9	2441.6	2105.3	1.04(29)		
379.9	2287.9	1907.7	0.52(19)		
483.5	2500.0	2017.6	0.44(5)		
508.0	2138.7	1630.7	–		
553.4	2568.9	2017.6	0.99(8)		
589.9	2220.6	1630.7	9.96(76)	0.10(3)	−0.14(5)
600.2	2196.8	1596.6	3.86(52)		
612.3	2208.8	1596.6	10.5(6)	0.03(2)	−0.07(3)
650.0	2245.5	1596.6	0.69(13)		
670.3	2017.6	1347.3	1.94(37)		
624.2	2220.6	1596.6	0.66(37)		
690.3	2287.9	1596.6	0.37(23)		
699.2	2279.8	1578.7	9.72(76)	0.004(20)	0.04(3)
722.4	2069.7	1347.3	<0.10		
727.7	2633.9	1907.7	1.10(21)		
757.8	2354.5	1596.6	–		
758.0	2105.3	1347.3	–		
768.4	2752.4	1984.8	–		
768.8	2088.4	1320.3	–		
769.8	2400.5	1630.7	–		
775.7	2096.0	1320.3	<0.10		
781.2	2797.3	2017.6	<0.10		
785.3	2105.3	1320.3	0.65(39)		
793.7	2700.6	1907.7	1.62(18)		
804.0	2400.5	1596.6	1.42(13)		
824.2	2421.1	1596.6	–		
824.9	1578.7	754.3	45.8(23)	0.02(2)	−0.004(26)
835.5	2183.7	1347.3	<0.10		
845.7	2752.4	1907.7	–		
847.3	2196.8	1347.3	–		
861.1	2208.8	1347.3	1.74(27)	0.04(10)	0.06(14)
863.5	2183.7	1320.3	0.96(11)		
873.6	2220.6	1347.3	<0.10		
888.1	2484.6	1596.6	4.76(38)	−0.06(5)	0.05(7)
898.1	2245.5	1347.3	–		
899.2	2219.5	1320.3	–		
902.5	2500.0	1596.6	–		
905.8	2484.6	1578.7	9.13(38)	0.05(6)	0.04(8)
907.5	2228.3	1320.3	–		
925.4	2245.5	1320.3	2.36(43)		
932.1	2279.8	1347.3	2.70(42)		
938.3	2568.9	1630.7	3.46(39)		
941.2	2287.9	1347.3	1.05(11)		
956.8	2553.5	1596.6	1.58(35)		
960.8	2279.8	1320.3	<0.10		
967.4	2287.9	1320.3	0.63(165)		
971.8	2568.9	1596.6	1.54(510)		

Table 1. Continued.

E_γ (keV)	E_i (keV)	E_f (keV)	I_γ	A_2/A_0	A_4/A_0
990.1	2568.9	1578.7	7.33(70)	−0.04(6)	−0.03(9)
1016.7	2363.9	1347.3	3.54(54)		
1034.3	2354.5	1320.3	1.97(82)		
1037.2	2633.9	1596.6	13.6(7)		
1043.7	2363.9	1320.3	3.16(39)		
1052.9	2400.5	1347.3	1.66(35)		
1065.2	1320.3	255.1	4.71(48)	0.15(2)	0.11(3)
1073.8	2421.1	1347.3	2.70(38)	0.47(12)	−0.07(15)
1080.2	2400.5	1320.3	3.34(40)		
1093.5	2441.6	1347.3	1.37(44)		
1104.1	2700.6	1596.6	5.62(78)	−0.07(5)	−0.09(6)
1121.4	2441.6	1320.3	2.39(25)	0.11(7)	0.12(10)
1142.2	2489.5	1347.3	10.7(12)		
1152.7	2500.0	1347.3	0.77(26)		
1155.5	2752.4	1596.6	–		
1173.5	2752.4	1578.7	3.36(41)		
1180.0	2500.0	1320.3	<0.10		
1193.9	2541.2	1347.3	17.0(8)		
1206.3	2553.5	1347.3	3.98(48)	−0.008(63)	0.15(9)
1221.4	2568.9	1347.3	3.52(43)		
1233.2	2553.5	1320.3	1.98(41)		
1236.0	2831.8	1596.6	–		
1240.1	2818.8	1578.7	18.8(11)	0.06(1)	−0.03(2)
1248.6	2568.9	1320.3	0.69(23)		
1250.9	2598.2	1347.3	1.52(31)		
1259.1	2606.4	1347.3	2.10(34)		
1270.6	2849.0	1578.7	2.26(30)		
1313.6	2633.9	1320.3	19.7(11)		
1320.3	1320.3	0.0	72.1(25)	−0.002(10)	−0.02(1)
1321.3	2900.0	1578.7	–		
1341.6	1596.6	255.1	4.54(51)		
1347.4	1347.3	0.0	100		
1353.3	2700.6	1347.3	2.62(57)		
1375.7	1630.7	255.1	9.08(72)		
1380.4	2700.6	1320.3	3.05(50)		
1429.7	2776.8	1347.3	2.07(32)		
1431.9	2752.4	1320.3	–		
1449.9	2797.3	1347.3	1.09(31)		
1456.3	2776.8	1320.3	1.45(36)		
1472.5	2818.8	1347.3	–		
1484.1	2831.8	1347.3	<0.10		
1502.2	2849.0	1347.3	–		
1511.5	2831.8	1320.3	0.92(37)		
1528.0	2849.0	1320.3	14.0(7)	−0.05(2)	−0.02(2)
1561.8	2909.0	1347.3	–		
1563.4	1818.5	255.1	5.56(55)		
1587.8	2909.0	1320.3	<0.10		
1596.6	1596.6	0.0	34.8(17)	−0.03(2)	−0.05(3)
1604.2	2951.5	1347.3	–		
1610.0	3188.7	1578.7	7.53(91)		
1630.7	1630.7	0.0	21.8(13)		
1631.4	2951.5	1320.3	–		
1633.4	3212.1	1578.7	–		
1652.6	1907.7	255.1	19.4(12)	−0.04(2)	−0.01(3)
1704.5	3051.9	1347.3	–		
1729.7	1984.8	255.1	17.1(10)	0.03(3)	0.02(5)
1732.0	3051.9	1320.3	–		
1793.7	3114.0	1320.3	8.84(69)	−0.04(6)	−0.01(9)
1814.5	2069.0	255.1	–		

Table 1. Continued.

E_γ (keV)	E_i (keV)	E_f (keV)	I_γ	A_2/A_0	A_4/A_0
1818.4	1818.5	0.0	4.36(294)	0.11(5)	−0.04(7)
1833.2	2088.4	255.1	0.60(40)		
1840.9	2096.0	255.1	–		
1841.9	3188.7	1347.3	–		
1880.3	3459.0	1578.7	2.61(39)		
1883.6	2138.7	255.1	4.00(48)		
1907.7	1907.7	0.0	11.0(7)	0.01(8)	0.08(10)
1928.6	2183.7	255.1	<0.10		
1948.5	3268.8	1320.3	3.44(70)		
1973.2	2228.3	255.1	4.69(90)		
2016.3	2016.3	0.0	19.4(9)	0.03(5)	−0.05(7)
2025.3	2279.8	255.1	0.58(34)		
2065.1	2818.8	754.2	2.66(60)	−0.31(5)	−0.29(7)
2088.4	2088.4	0.0	7.00(69)	0.03(3)	0.003(35)
2104.9	2105.3	0.0	8.58(68)	0.02(8)	0.03(12)
2109.0	2363.9	255.1	–		
2136.9	2392.0	255.1	3.68(56)		
2175.5	3523.2	1347.3	4.12(53)		
2203.9	3523.2	1320.3	1.84(29)		
2244.9	2500.0	255.1	11.8(9)		
2296.3	2551.4	255.1	2.11(41)		
2363.8	2363.9	0.0	8.63(107)		

two kinds of matrices. One was the usual symmetric γ-γ matrix, with gamma-ray energy on both axes. The second one was a "two-step cascade" (TSC) matrix, with the γ-ray energy on one axis, and the sum of the energies of any two coincident gamma rays on the other axis. The use of the TSC matrix helps very much in the coincidence relationship analysis, since in the $(\mathrm{p},\mathrm{n}\gamma)$ reaction the final states have relatively low excitation energy and consequently decay towards the ground state by a small number of gamma-ray transitions. Thus, a level which decays by one or more cascades of two transitions to the ground state or to an isomeric state will show up as a peak on the sum energy axis, whose energy has a direct relationship to the excitation energy of that level; gating on such a peak, all two-step γ-ray cascades implied in its decay will appear in a typical, symmetric spectrum, containing all pairs of the corresponding gamma transitions. The coincidences observed in this way can also be cross-checked by gating on the usual symmetric γ-γ coincidence matrix.

A second type of measurement has been performed at 5.0 MeV incident energy, in the singles mode, by keeping one of the Ge detectors at 90° and moving the second one in 10 steps, equidistant in $\cos\theta$, between 15° and 143°. This measurement has been performed for both gamma-ray angular distribution and Doppler shift attenuation purposes; the stability of the electronics has been monitorized by keeping a ^{60}Co source near the target during the measurements.

2.2 The ^{130}Te(^{12}C, 3nγ)^{139}Ce reaction study

In this experiment, a beam of $^{12}C^{6+}$ with energy of 50.5 MeV and an intensity of about 5 particle nA has been delivered also by the tandem accelerator of our Institute. The target was enriched in ^{130}Te (99.1%) and was 2.25 mg/cm^2 thick. The γ-rays have been detected with three 25% HPGe detectors placed at angles of 15°, 90°, and 125° with respect to the beam, at a distance of 10 cm from the target. The coincidences between these three detectors have been registered on-line, and then sorted off-line in two different matrices: a usual symmetric γ-γ one, and a non-symmetric one, with the energy of the detectors from 90° and 125° on the two axes, respectively. The non-symmetric matrix was used to deduce DCO (directional correlation orientation) ratios for multipolarity assignments.

3 Experimental results

3.1 States with low spin and excitation energy

3.1.1 Level scheme

Here we present the results of the $(\mathrm{p},\mathrm{n}\gamma)$ experiment. Figures 1 and 2 show the level and γ-ray decay scheme of ^{139}Ce as observed from these measurements. Associated information is provided in table 1, which contains a list of the energies and intensities of all γ-ray transitions assigned to levels of ^{139}Ce, as well as the Legendre polynomial coefficients A_2/A_0 and A_4/A_0 obtained from the angular distributions for the stronger transitions. This level scheme has been obtained on the basis of the coincidences with the neutrons, and of the γ-γ coincidence relationships. For the levels in table 1 and figs. 1 and 2, for which more than one de-excitation gamma-ray path was found, the adopted excitation energy corresponds to a weighted average of

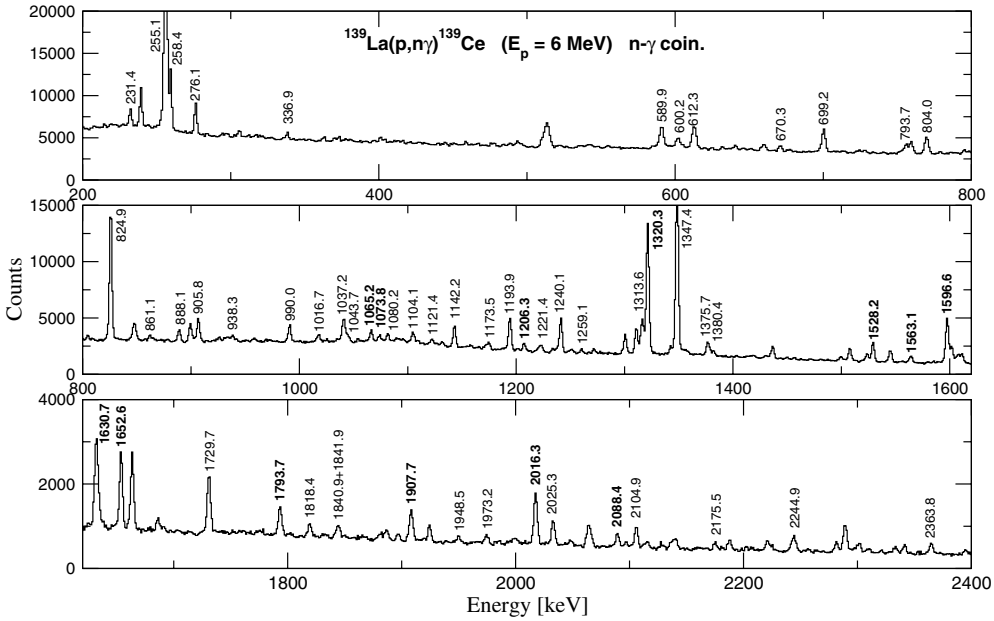

Fig. 3. Gamma-ray spectrum coincident with the neutrons, in the ^{139}La(p, nγ) reaction at $E_p = 6$ MeV. The strongest peaks assigned to the level scheme of ^{139}Ce (figs. 1, 2) are labeled with their energy in keV. The γ-rays for which Doppler shifts could be observed (see sect. 3.1.2) are labeled with bold characters.

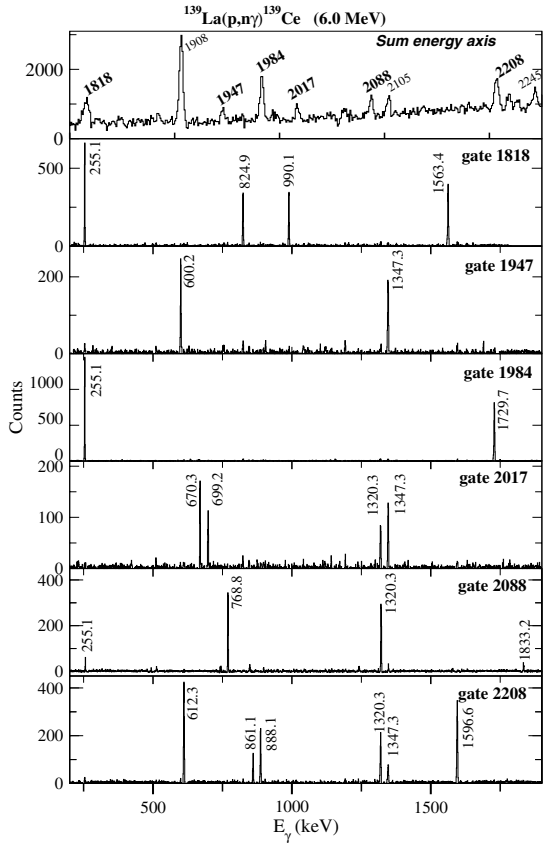

Fig. 4. Examples of gates set on the sum energy axis of the TSC (two-step cascade) γ-γ coincidence matrix of the (p, nγ) reaction data. The upper panel shows a portion of the sum energy axis. Gates on the peaks labeled with their energy (in keV) are shown in the subsequent panels (for details, see text).

the values determined from the different paths. Some examples of the analysis of the coincidences are given in figs. 3, 4, and 5.

Figure 3 shows the spectrum of the γ-rays coincident with neutrons. Since the (p, 2n) reaction channel opens only at energies above 10 MeV, and the target has a high purity, most of the γ-rays observed in this spectrum correspond to the (p, n) channel, *i.e.*, ^{139}Ce. The strongest γ-rays in this spectrum, which have been assigned to the level scheme of ^{139}Ce (figs. 1 and 2), are labeled by their energies (see also table 1). This spectrum is important especially in establishing transitions from excited states to the ground state. The relative intensities of the transitions from table 1 are extracted from this spectrum.

Figure 4 gives some examples of analysis based on the TSC matrix. The upper panel shows a portion of the sum energy axis, and the next panels are γ-ray spectra obtained by setting gates on the peaks in the first panel which are labeled by their energy. These panels illustrate different possible situations. Thus, in the "gate 1818" panel one observes one pair of gammas (255 and 1563 keV) which decays from the 1818 keV level to the ground state, and a second pair of gammas (825 and 990 keV) whose sum is close to 1818 (and therefore was included in the gate) and come from the decay of the 2569 keV level (fig. 2) which ends on the known isomeric level at 754 keV [1]. The panel "gate 1947" shows one pair of coincident gammas which originates from the decay of the 2197 keV level; "gate 1984" shows the only cascade which de-excites the level with the same energy; "gate 2017" is similar to "gate 1818", showing one pair (670.3 and 1347.3 keV) which de-excites the 2017 keV level to the g.s., and another coincident pair with approximately the same sum energy which de-excites the 2280 keV level; "gate 2088" shows the two

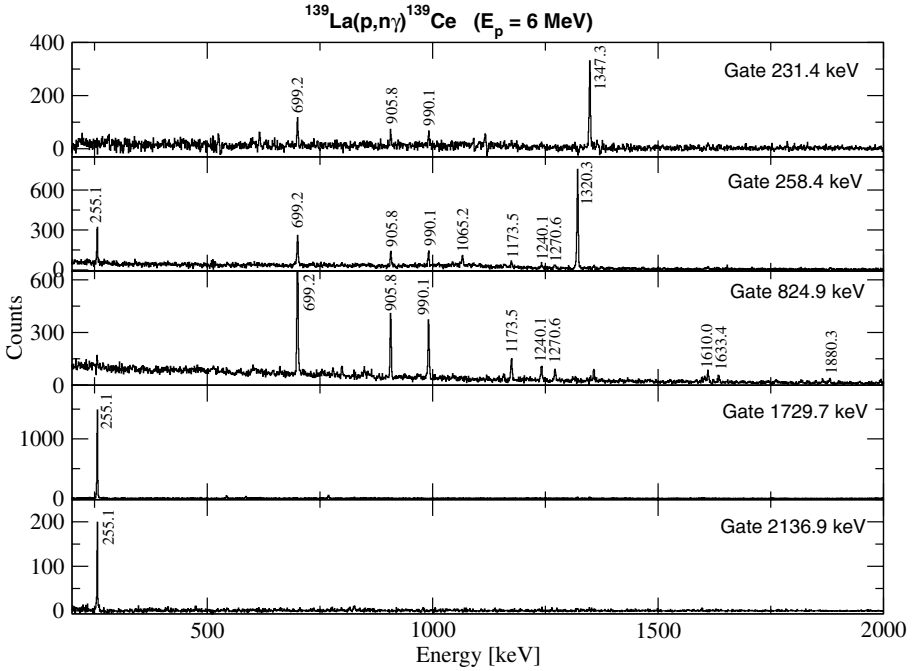

Fig. 5. Some examples of gates from the symmetric γ-γ coincidence matrix (the $(p, n\gamma)$ reaction data).

cascades which de-excite the 2088 keV level to the g.s., and, finally, "gate 2208" shows the decay of the level at 2208 keV which decays to the ground state by three different two-step cascades.

Figure 5 shows examples of gates obtained from the symmetric γ-γ coincidence matrix. The first three spectra are gated by the transitions found to de-excite the 1578.7 keV negative-parity level, for which only the 824 keV transition has been tentatively assigned in the previous, non-coincident studies [1]; the 258 keV gate shows also the existence of the 1065.2 keV branch of the 1320.2 keV level [1]. All these three gates show in addition a number of transitions which define the de-excitation of different levels placed above the 1578.7 keV level (see figs. 1, 2). The lowest two spectra in fig. 5 illustrate the levels assigned at 1985 keV and 2392 keV, respectively, which were found to decay only to the 255 keV level through the transitions of 1730 and 2137 keV, respectively (see also fig. 1).

Figures 1, 2 and table 1 show that a total number of 49 levels have been assigned above the excitation energy of 2 MeV. Since the (p, n) reaction is non-selective, it is likely that up to about 3 MeV excitation all levels with spin lower than $\sim 11/2$ have been observed. Above 3 MeV the density of states is larger and we have assigned only a few, more strongly populated levels. Many of these levels coincide with levels proposed from the beta decay [2] or transfer reaction studies [4] (see also [1] and references therein). Practically all adopted levels above 2.5 MeV excitation [1] have been observed before only in the transfer reaction studies [4,1]; within the quoted accuracy of 10 keV for their excitation energy [4], many of these levels appear to have been observed in this work. This is shown in table 2 which lists the levels found in the present work, and, when existing, their correspondence with the levels known before [4,1]. Thus, most of the levels proposed from the transfer reaction studies have been confirmed by our $(p, n\gamma)$ reaction study. In general, the measured gamma-ray angular distributions are rather flat (see the Legendre polynomial coefficients in table 1) therefore new multipolarity assignments could not be proposed with sufficient accuracy. In the cases where a larger asymmetry was observed, the known multipolarities [1] of the transitions (cf. table 2) are confirmed.

3.1.2 Lifetime determinations

The spectra measured at different angles could be used to obtain information on the lifetimes of some of the levels populated in the $(p, n\gamma)$ reaction using the Doppler shift attenuation method (DSAM). At the incident energy of 5 MeV we are not so far from the threshold of exciting the levels around 2 MeV, therefore the recoiling nuclei can still be approximated as moving forward within a narrow cone, with an average velocity equal to that of the centre of mass. The recoil velocity is very small, therefore leading to small shifts of the gamma-ray energy but still measurable. The stability of the electronics has been checked by verifying the position of the peaks due to the ^{60}Co source, background lines (such as 1460.8 keV of ^{40}K), or lines from ^{139}Ce known to come from levels with long lifetime, or found from the analysis to present no shift. The centroid of a peak representing a transition from a level whose lifetime is comparable with the stopping time of the recoil nucleus into the target material will vary linearly with the cosine of the detection angle (with respect to the

Table 2. Excitation energies of the levels observed in the present $(\mathrm{p},\mathrm{n}\gamma)$ reaction study, compared to the levels known before [1]. The previously known levels above 2500 keV are those from transfer reactions (mainly (d,t), see also [4]). The "high-spin" levels, observed in the $(\alpha, x\mathrm{n})$ reaction study [5] and the present $(^{12}\mathrm{C}, 3\mathrm{n}\gamma)$ reaction study, are not shown in this table and will be discussed later.

Present exp.	Previous [1]	
E_x (keV)	E_x (keV)	J^π
255.1	255.098	$1/2^+$
754.2	754.24	$11/2^-$
1320.3	1320.249	$5/2^+$
1347.3	1347.337	$7/2^+$
1578.7	1578.25?	$7/2^-$
1596.6	1596.590	$(3/2^+)$
1630.7	1630.681	$3/2^+$
	1790?	$(1/2^+)$
1818.5	1818.49	$3/2^+$, $5/2^+$
	1842.9?	$(7/2^-)$
	1889	$1/2^+$
1907.7	1907.679	$(3/2^+)$
	1965.38	3/2, $5/2^+$
1984.4	1984.86	3/2, $5/2^+$
2016.3	2016.27	$(3/2^+)$
2017.6		
	2028.6	$(11/2^-, 13/2)$
2069.7		
2088.4	2090.5	3/2, $5/2^+$
2096.0		
2105.3		
2138.7	2143	3/2, $5/2^+$
2183.7		
2196.8		
2208.8		
2219.5		
2220.6		
2228.3		
2245.5	2251	$7/2^+$
2279.8		
2287.9	2286	$(7/2^+, 9/2^\pm, 11/2^-)$
2354.5		
2363.9	2363	$7/2^+$, $9/2^+$
2392.0		
2400.5		
2421.5	2426	3/2, $5/2^+$
2441.6		
	2455	$7/2^+$, $9/2^+$
2484.5	2483.6?	
2489.5	2488	
2500.0		
2541.2		
2551.4		
2553.5	2556	$(7/2, 9/2)^+$
2568.9		
2598.2		
2606.4	2610	
2633.9		
2700.6	2701	
2752.4		
2776.8		
2797.3	2800	$7/2^+$, $9/2^+$
2818.8	2822.5	$9/2^-$, $11/2^-$
2831.8		
2849.0		
2900.0		
2909.0	2910	$3/2^+$, $5/2^+$ and $9/2^+$
2951.5		
	2964	$3/2^+$, $5/2^+$
3051.9		
	3082	$(7/2^+, 9/2^+)$
3114.0		
	3144	$1/2^+$
	3172?	$3/2^+$, $5/2^+$
3188.7	3196	$(7/2^+, 9/2^+)$
3212.1		
3268.8		
	3282	$7/2^+$, $9/2^+$
	3302	$1/2^+$
3459.0		
3523.2		

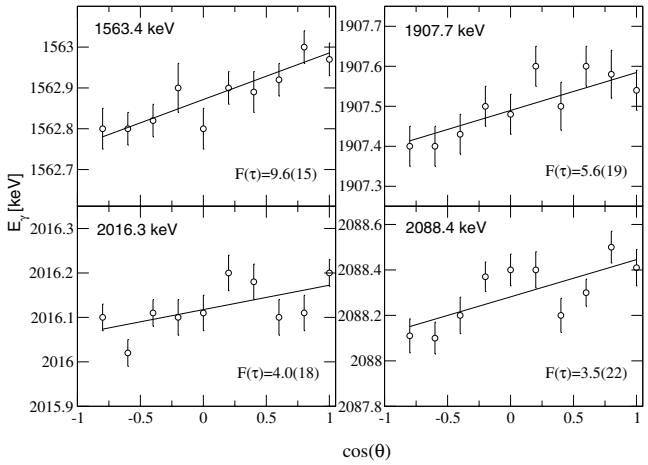

Fig. 6. Illustration of the attenuated Doppler shifts observed for some γ-rays in the $(\mathrm{p},\mathrm{n}\gamma)$ reaction at 5.0 MeV. The peak centroid energies represented in these graphs are those measured relatively to the closest unshifted peak, using a local linear calibration, so their average may differ somewhat from the adopted γ-ray energy (table 1, figs. 1 and 2). However, the relative energies at different angles, which count in measuring the slope of the linear variation with $\cos\theta$ ($\sim F(\tau)$) are correct.

recoil direction) —the "centroid" variant of the DSAM:

$$E_\gamma(\theta) = E_0\left(1 + \frac{\tilde{v}}{c}F(\tau)\cos\theta\right).$$

We could detect shifts for a number of gamma rays from our spectra (these transitions are indicated in bold numbers in fig. 3). Figure 6 shows some examples of such measured attenuated Doppler shifts. From the slopes of the linear fits one determines the experimental attenuated shifts $F(\tau)$, which can be compared to calculated

Table 3. Level lifetimes measured with the DSAM method in the (p, nγ) reaction at 6.0 MeV incident energy. The attenuated shifts $F(\tau)$ lead to the lifetime values labeled "Effective τ". The levels 1320.3, 1596.6, and 1630.7 keV have large feedings from higher levels (see table 1), therefore the effective lifetime is taken as an upper limit of the level lifetime. For the rest of the levels the feeding from above is negligible, therefore the adopted lifetime coincides with the effective one.

E_{level} (keV)	E_γ (keV)	$F(\tau)$ (%)	Effective τ (ps)	Adopted τ (ps)
1320.3	1320.3	6.6(16)	$1.0^{+0.5}_{-0.3}$	< 1.5
	1065.2	6.6(33)	$1.0^{+1.8}_{-0.4}$	
1596.6	1596.6	7.7(20)	$0.86^{+0.41}_{-0.22}$	< 1.3
1630.7	1630.7	5.5(32)	$1.3^{+4.2}_{-0.6}$	< 5.5
1818.5	1563.4	9.6(15)	$0.65^{+0.16}_{-0.11}$	$0.65^{+0.16}_{-0.11}$
1907.7	1907.7	5.6(19)	$1.3^{+1.1}_{-0.4}$	1.7(8)
	1652.6	5.0(21)	$1.5^{+2.1}_{-0.6}$	
2016.3	2016.3	4.0(!8)	$2.0^{+4.2}_{-0.8}$	< 6.2
2088.4	2088.4	3.5(22)	> 1.2	> 1.2
2421.5	1073.8	10.0(39)	$0.62^{+0.54}_{-0.21}$	$0.62^{+0.54}_{-0.21}$
2553.5	1206.3	8.8(31)	$0.72^{+0.54}_{-0.22}$	$0.72^{+0.54}_{-0.22}$
2849.0	1528.0	7.3(1.5)	$0.91^{+0.31}_{-0.19}$	$0.91^{+0.31}_{-0.19}$
3114.0	1793.7	6.2(16)	$1.14^{+0.60}_{-0.30}$	$1.14^{+0.60}_{-0.30}$

values, in order to obtain τ, the level lifetime. Besides the experimental error in determining the $F(\tau)$ value, the resulting error in τ is dominated by the uncertainties in the stopping power used to calculate the slowing down of the recoiling nuclei. As in previous applications of the DSAM in the (p, nγ) reaction (see, *e.g.*, [7]) we have used the LSS electronic stopping-power theory [8], and the formalism of Blaugrund [9] for the nuclear stopping power in calculating the theoretical $F(\tau)$-function. Table 3 gives the information extracted in this way for the transitions for which some Doppler shift could be evidenced. In general, the observed shifts are quite small ($F(\tau)$ values smaller than 10%); in this range, and with the measured uncertainties, the errors resulting for the lifetimes are usually quite large and asymmetric. The lower levels, at 1320.3, 1596.6, and 1630.7 keV have considerable feedings from the higher levels (see fig. 1 and table 1), therefore their "effective" lifetime deduced from the $F(\tau)$ value represents only an upper limit of the level lifetime. The rest of the levels have very small feeding from above (*e.g.*, 1907.7 keV level —about 10%), or no such feeding, therefore the adopted τ is equal to the "effective" one and is presented in the last column. Reduced electromagnetic transition probabilities determined from these lifetimes for some of the lower levels are given in table 4.

3.2 High-spin states

Figure 7 shows the high-spin level scheme observed in the present ^{130}Te(^{12}C, 3n) reaction experiment. This level scheme has been constructed by observing the gamma-ray

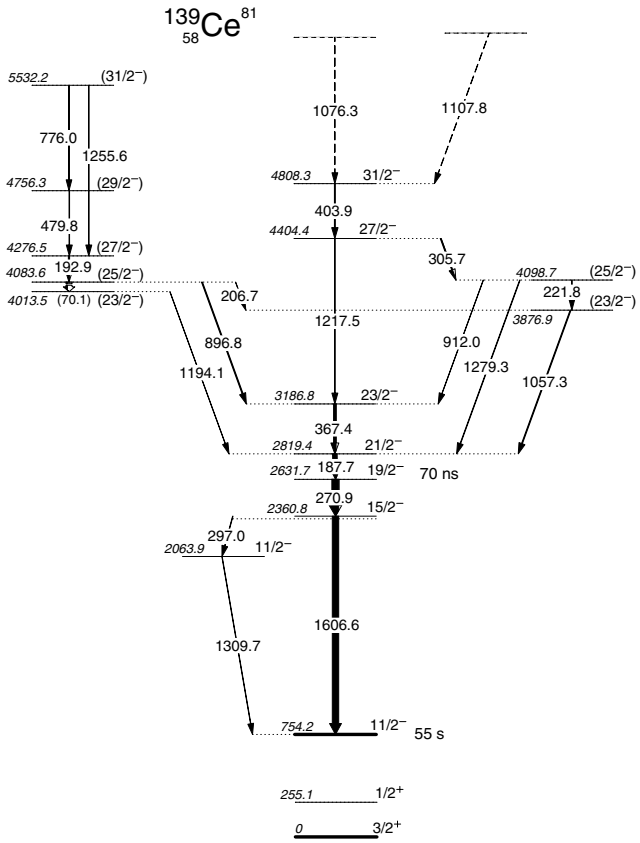

Fig. 7. High-spin level scheme of ^{139}Ce, as observed in the present ^{130}Te(^{12}C, 3nγ) experiment.

coincidence relationships (gates on the symmetric γ-γ matrix), starting from the known 1607 keV transition which has been assigned to directly populate the 754 keV, $11/2^-$ isomeric state [5,6], and taking into account the intensity balances. Multipolarities for the observed transitions have been determined by using DCO ratios deduced from the asymmetric matrix constructed from the two detectors at 90° and 125°. For a pure quadrupole transition, this DCO ratio should be about 1.0 when gating on a quadrupole transition and about 2.0 when gating on a stretched dipole one, while for a pure dipole transition it is about 1.0 and 0.5 when gating on a dipole or a quadrupole transition, respectively.

Table 5 gives the transitions assigned to the decay of the high-spin states observed in this experiment with their intensity, DCO ratio, and assignment in the level scheme. For all stronger transitions, DCO ratio values have been determined with different gating transitions, starting from gates on lower transitions of known multipolarity [5] (in table 5 only one determination is given, as an example, for each transition), and one can see that these DCO ratio values define rather consistently the spin values assigned to the observed states. In assigning these spin values, one has started from the values assigned to the lower states in the previous work [5], and it was assumed that the spins generally increase with excitation energy. We have also assumed that the transitions with quadrupole mul-

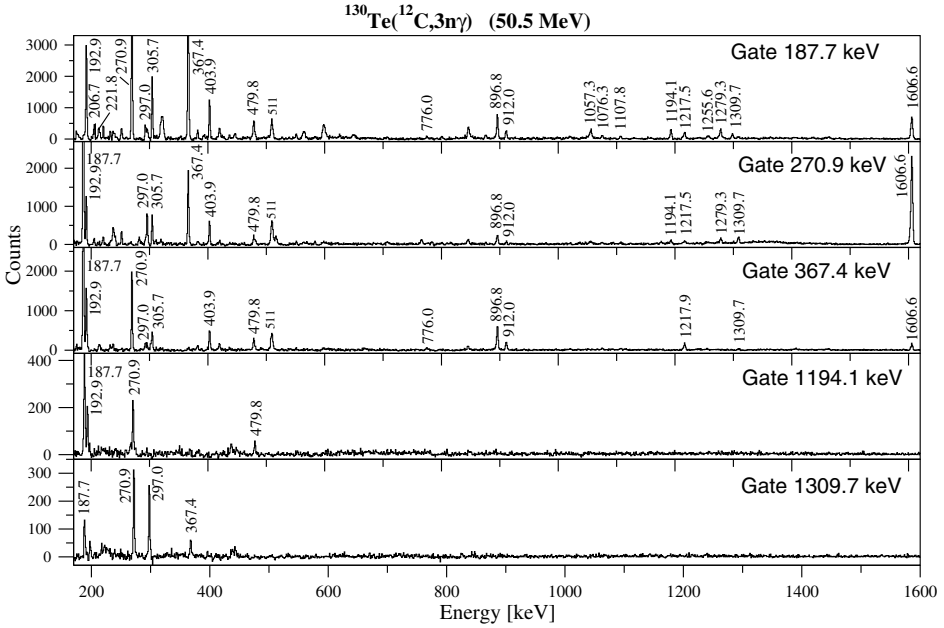

Fig. 8. Some examples of gated spectra obtained from the symmetric γ-γ matrix for the ^{130}Te(^{12}C, 3nγ) reaction, illustrating the level scheme of fig. 7.

Table 4. Reduced electromagnetic transition probabilities resulted from lifetimes reported in this work (table 3) for some of the lowest levels. When the multipolarity (mixing ratio) of the transition is not known, both the $B(E2)$ and $B(M1)$ value for a pure transition are given.

τ (ps)	E_i (keV)	J_i^π	E_f (keV)	J_f^π	E_γ (keV)	Br. ratio %	$B(E2)$ (W.u.)	$B(M1)$ (mW.u.)
< 1.5	1320.3	$5/2^+$	g.s.	$3/2^+$	1320.3	100(1)	> 2.9	> 8.6
			255.1	$1/2^+$	1065.0	6.1(7)	> 0.6	
< 1.3	1596.6	$(3/2^+)$	g.s.	$3/2^+$	1596.6	100(5)	> 1.1	> 4.6
			255.1	$1/2^+$	1341.6	13.0(15)	> 0.3	> 1.0
			1320.3	$5/2^+$	276.1	14.5(5)	> 960	> 123
			1347.3	$7/2^+$	249.3	< 0.3	> 33	> 3.5
< 5.5	1630.7	$3/2^+$	g.s.	$3/2^+$	1630.7	100(6)	> 0.2	> 0.9
			255.1	$1/2^+$	1375.7	41.7(33)	> 0.2	> 0.6
			1320.3	$5/2^+$	310.7	0.7(3)	> 3.3	> 0.6
			1347.3	$7/2^+$	283.7	1.5(6)	> 11.6	
0.68(13)	1818.5	$3/2^+, 5/2^+$	g.s.	$3/2^+$	1818.4	79(6)	0.6(3)	3.3(15)
			255.1	$1/2^+$	1563.4	100(10)	1.6(6)	6.7(24)
1.7(8)	1907.7	$(3/2^+)$	g.s.	$3/2^+$	1907.7	56(4)	0.16(7)	1.0(4)
			255.1	$1/2^+$	1652.6	100(6)	0.6(3)	2.6(12)

tipolarity are of electric type, and the dipole ones are of magnetic type. The lowest states, which decay to the isomeric $11/2^-$ level, belong to the $h_{11/2}$ excitation family, therefore have negative parity. Up to the state 3187 keV, $23/2^-$, the (yrast) level scheme coincides with that determined in ref. [5], except for the $11/2^-$ state which is found at 2064 keV. Above the $23/2^-$ state, the yrast line is observed up to a $(31/2^-)$ state. A rather regular band-like structure with $\Delta J = 1$, based on a $J = (23/2)$ state at 4014 keV is also found which, due to its prompt decay to the yrast negative-parity states, is tentatively assigned as having negative parity too.

Figure 8 shows some examples of observed γ-γ coincidences. While the first three gates illustrate the connections of the yrast line with the other two structures shown in fig. 7, the fourth gate (1194.1 keV) shows that the 1194.1 keV transition "sees" those of 192.9 and 479.8 keV, thus indicating the presence of the 70.1 keV transition which was not observed due to both its large internal conversion coefficient and its proximity to our electronic cutoff. The fifth panel (gate on the 1309.7 keV transition) shows that the 1309.7-297.0 cascade bypasses the 1606.6 keV transition. The position of the 2064 keV level was chosen according to systematics in this mass region.

Table 5. Information on the high-spin states observed in ^{139}Ce with the (^{12}C, 3nγ) reaction. For the DCO ratio values given in the table, the gating transition is specified.

E_γ (keV)	E_i (keV)	E_f (keV)	I_γ	R_{DCO}	Gate[a]	J_i^π	J_f^π
(70.1)[b]	4083.6	4013.5	–	–	–	$(25/2^-)$	$(23/2^-)$
187.7(1)	2819.4	2631.7	56.3(17)	0.68(7)	C	$21/2^-$	$19/2^-$
192.9(1)	4276.5	4083.6	15.3(11)	0.85(12)	B	$(27/2^-)$	$(25/2^-)$
206.7(2)	4083.6	3876.9	2.5(4)			$(25/2^-)$	$(23/2^-)$
221.8(2)	4098.7	3876.9	3.3(10)	1.13(21)	B	$(25/2^-)$	$(23/2^-)$
270.9(2)	2631.7	2360.8	100(5)	1.96(22)	B	$19/2^-$	$15/2^-$
297.0(1)	2360.8	2063.9	5.9(3)	0.87(18)	A	$15/2^-$	$11/2^-$
305.7(1)	4404.4	4098.7	11.9(5)	0.88(11)	B	$(27/2^-)$	$25/2^-$
367.4(1)	3186.8	2819.4	36.4(9)	1.23(11)	B	$23/2^-$	$21/2^-$
403.9(1)	4808.3	4404.4	12.8(12)	1.92(32)	B	$31/2^-$	$27/2^-$
479.8(1)	4756.3	4276.5	7.2(15)	0.67(23)	B	$(29/2^-)$	$(27/2^-)$
776.0(1)	5532.2	4756.3	3.1(7)	0.96(30)	D	$(31/2^-)$	$(29/2^-)$
896.8(1)	4083.6	3186.8	13.8(7)	1.14(25)	B	$(25/2^-)$	$23/2^-$
912.0(2)	4098.7	3186.8	3.7(5)	0.81(23)	C	$(25/2^-)$	$23/2^-$
1057.3(2)	3876.9	2819.4	12.5(8)			$(23/2^-)$	$21/2^-$
1076.3(3)	5884.6	4808.3	5.2(6)				
1107.8(7)	5916.1	4808.3	4.4(4)				
1194.1(2)	4013.5	2819.4	3.4(12)	1.74(34)	B	$(23/2^-)$	$21/2^-$
1217.5(2)	4404.4	3186.8	7.7(10)	1.50(40)	B	$27/2^-$	$23/2^-$
1255.6(2)	5532.2	4276.5	7.5(21)			$(31/2^-)$	$(27/2^-)$
1279.3(2)	4098.7	2819.4	7.5(14)	1.52(28)	B	$(25/2^-)$	$21/2^-$
1309.7(2)	2063.9	754.2	5.4(3)	1.48(6)	A	$11/2^-$	$11/2^-$
1606.6(2)	2360.8	754.2	94.3(42)	1.78(25)	B	$15/2^-$	$11/2^-$

[a] Gating transition: A: 270.9 keV (quadrupole); B: 187.7 keV (dipole); C: 367.4 keV (dipole); D: 192.9 keV (dipole).
[b] Not directly observed.

4 Discussion and conclusions

One of the first interpretations of the structure of ^{139}Ce, and of other $N = 81$ nuclei, was made on the basis of the unified model, in which one neutron hole is coupled to quadrupole vibrations of the core [10]. The odd-neutron hole was allowed to occupy the $2d_{3/2}$, $3s_{1/2}$, $1h_{11/2}$, $1g_{7/2}$, and $2d_{5/2}$ states, and up to three quadrupole phonons have been considered for the even-even core. Below 1 MeV of excitation energy all these nuclei have almost pure $2d_{3/2}$, $3s_{1/2}$, and $1h_{11/2}$ neutron-hole states, as confirmed by the transfer reaction studies [4]. Reference [10] gives detailed predictions for the levels below 2 MeV excitation energy (electromagnetic transition probabilities, branching ratios). For the $1/2^+$ isomeric level at 255 keV the predicted half-life is 500 ps, compared to the experimental value of 110 ps [1]. For the $5/2_1^+$ state at 1320 keV, the lifetime is of 0.056 ps, while experimentally we have determined only an upper limit, $\tau < 1.5$ ps; the two branchings of this state, towards the $1/2^+$ state at 255 keV, and the $3/2^+$ ground state, are predicted with relative values of 1, and 0.066, respectively, in good agreement with the measured values (table 1) of 1 and 0.061, respectively. However, many of the spin-parity assignments of these low-lying states are different than the ones obtained in the calculations in [10], since they have been changed meanwhile (see ref. [1] and table 2). In addition, the mentioned unified model calculations predict one $1/2^+$ state, two $3/2^+$ states, two $5/2^+$ states, and one $7/2^+$ state, respectively, below 2 MeV, while experimentally the number of observed states is much larger (ref. [1], fig. 1 and table 2). The excess of levels with respect to the neutron-hole vibration model may be accounted for by taking into account other excitations of the ^{140}Ce core, as remarked in ref. [2]. A reasonably realistic shell model calculation for ^{139}Ce would require a very large configuration space. Though spin ambiguities could not be resolved in the present work, the decay scheme of many levels has been better specified, which will enable a better comparison with new model calculations. Thus, for the levels at 1579, 1597, 1631 keV, more branchings have been established, while for the levels at 1819, 1908, 1985, and 2016 keV some of the doubtful branches have not been confirmed, as it can be seen by a comparison of the data in table 1 and fig. 1 with those in ref. [1]. In addition, lifetimes (table 3) and electromagnetic transition probabilities (table 4) have become available.

For the high-spin levels obtained in the heavy-ion fusion-evaporation reaction, we show in fig. 9 a comparison with the known energy levels in the core nucleus ^{140}Ce [11,12]. Up to about 4.3 MeV exitation energy, the positive-parity states in ^{140}Ce are understood by shell model calculations within the proton space $(g_{7/2}, d_{5/2})^{Z-50}$, $(g_{7/2}, d_{5/2})^{Z-51}(d_{3/2}, s_{1/2})^1$ [11,12]. The negative-parity states require one-proton excitation in the $h_{11/2}$ shell, and since the diagonalization space becomes too large, they were treated by a truncation procedure within a particle-core model in which ^{139}La (the "core") is treated by a shell model description of the positive-parity

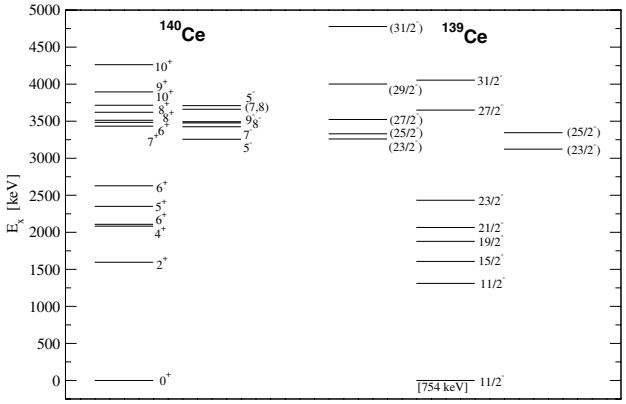

Fig. 9. Comparison between the level schemes of ^{139}Ce and ^{140}Ce.

states, and then the particle-core Hamiltonian is diagonalized in a basis of one $h_{11/2}$ proton coupled to known states of the core [11,12].

The similarity of the level scheme observed for ^{139}Ce with that of ^{140}Ce (fig. 9) suggests an explanation in terms of the coupling of one neutron to the states of the core. Such calculations have been performed in ref. [5], both by a weak or intermediate coupling of neutron holes in $h_{11/2}, d_{3/2}$, and $s_{1/2}$ to the vibrational states of the core, which account well for the observed negative-parity states up to the $23/2^-$ state at 3187 keV, as states resulting from the multiplets $(2^+ \otimes \nu h_{11/2}^{-1})$, $(4^+ \otimes \nu h_{11/2}^{-1})$, and $(6^+ \otimes \nu h_{11/2}^{-1})$. States at higher excitation energies should be of three-quasiparticle nature, and some of these states in both ^{139}Ce and ^{141}Nd have been described by coupling three particles (two $d_{5/2}$ protons and one $h_{11/2}$ neutron hole) to the ^{140}Ce core. A comparison with the experimental states for ^{139}Ce was shown only up to the known $23/2^-$ state at 3187 keV [5], while for the higher ^{141}Nd states it was concluded that the space should be enlarged by including other proton states as well. The structure observed above the 4014 keV state assigned as $(23/2^-)$ appears as a rotational band, therefore built on a deformed state. It would be interesting to confirm the deformation by measurements of the lifetimes of states in this band, and understand its microscopic origin.

References

1. T.W. Burrows, Nucl. Data Sheets **92**, 623 (2001).
2. M.R. Zalutsky, E.S. Macias, R.A. Meyer, Phys. Rev. C **13**, 1590 (1976).
3. M.B. Chatterjee, Phys. Rev. C **38**, 625 (1988).
4. G. Berrier, M. Vergnes, G. Rotbard, J. Kalifa, J. Phys. (Paris) **37**, 311 (1976).
5. J. Ludziejewski, H. Arnold, Z. Phys. A **281**, 287 (1977).
6. J. Ludziejewski, J. Bialkowski, Z. Haratym, L.-E. De Geer, A. Kerek, J. Kozyczkowski, Phys. Scr. **14**, 133 (1976).
7. M. Ivaşcu, N. Mărginean, I. Căta-Danil, C.A. Ur, Yu.N. Lobach, Phys. Rev. C **60**, 024302 (1999).
8. J. Lindhard, M. Scharff, H.E. Schiott, Mat.-Fys. Medd. K. Dan. Vidensk. Selsk. **33**, No. 14 (1963).
9. A. Blaugrund, Nucl. Phys. **88**, 501 (1966).
10. K. Heyde, P.J. Brussaard, Z. Phys. A **259**, 15 (1973).
11. W. Enghardt, H.U. Jäger, L. Käubler, H.-J. Keller, H. Prade, F. Stary, Z. Phys. A **316**, 245 (1984).
12. W. Enghardt, H. Prade, H.U. Jäger, L. Käubler, H.-J. Keller, F. Stary, Ann. Phys. (Leipzig) **43**, 424 (1986).